

# String-to-Battery Voltage Equalizer Based on Half-Bridge Converter with Multi-Stacked Current Doublers for Series-Connected Batteries

Masatoshi Uno, *Member, IEEE*, and Akio Kukita

**Abstract**— Voltages of series-connected batteries gradually become imbalanced due to non-uniformity in terms of not only battery characteristics but also self-discharge rate that is significantly dependent on temperature. In large-scale energy storage systems, a large temperature gradient is very likely because of its huge geometry, and therefore, equalizers capable of relatively large equalization currents would be necessary to eliminate voltage imbalance originating from uneven temperature distribution. A two-switch string-to-battery voltage equalizer using a half-bridge converter with multi-stacked current doublers (MSCDs) is proposed for series-connected batteries in this paper. The proposed equalizer is capable of providing relatively large equalization currents without increasing ripple currents thanks to the interleaved operation of the MSCDs. Fundamental operational analysis for discontinuous conduction mode (DCM), in which currents in the equalizer can be limited to desired levels without feedback control, is performed. The experimental results of equalization tests performed for four supercapacitor modules and lithium-ion batteries connected in series demonstrated the equalization performance of the proposed equalizer.

**Index Terms**— Current doubler, discontinuous conduction mode (DCM), lithium-ion battery, supercapacitor, voltage equalizer, voltage imbalance

## I. INTRODUCTION

IN a battery string comprising series-connected energy storage cells/modules/batteries (hereafter, simply call batteries unless otherwise noted), including lithium-ion batteries and supercapacitors (SCs), the voltage mismatch among them gradually grows due to non-uniform individual battery characteristics in terms of capacity, self-discharge rate, and internal impedance. In general, the higher the voltage, the sooner the batteries deteriorate. Therefore, each battery in a voltage-mismatched string ages unevenly, resulting in accelerated aging of the system as a whole. Furthermore, since all batteries in the string are charged/discharged in series, some batteries with higher/lower voltages might be over-charged/-discharged during the charging/discharging process, potentially triggering hazardous consequences of a fire or, in the worst case, an explosion. Voltage equalization is thus indispensable for

battery strings to ensure years of safe operation and to optimally exploit battery performance and its stored energy.

In recent applications of energy storage systems such as electric vehicles, the physical size of systems is upsizing to meet large power requirement. For such large-scale systems, modular architectures are often employed—batteries or modules, each consisting of several cells connected in series, are stacked in series to form a system. A temperature gradient in a system is prone to be significant as the size of the system increases, as illustrated in Fig. 1. The larger the system size, the greater will be the temperature gradient among batteries. Meanwhile, cell temperatures in each battery pack comprising several cells connected in series can be relatively easily evened because of its relatively small geometry. The temperature gradient in a system generates cumbersome issues as self-discharge rate is significantly dependent on temperature—self-discharge is accelerated at high temperatures (roughly doubled for every 10°C increase according to Arrhenius Law), and thus voltage imbalance is prone to be exacerbated due to non-uniform self-discharge. Achieving uniform temperature distribution in battery systems, however, is a daunting challenge even with sophisticated thermal designs [1], [2]. Needless to say, worse temperature gradients are very likely with unsophisticated thermal designs. For example, if batteries are placed near both an engine and radiator in a plug-in hybrid electric vehicle with unsophisticated thermal design, the temperature gradient in the battery system would be exacerbated.

In modular architectures, battery- and cell-level equalizers are separately used [3]–[5] to effectively preclude voltage

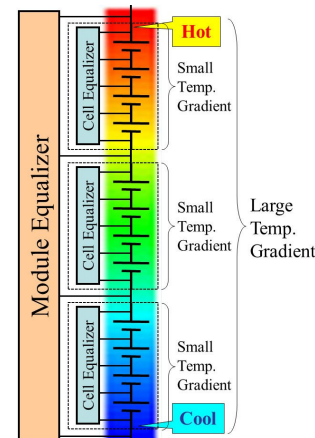


Fig. 1. Temperature gradients in energy storage systems based on modular architecture.

Manuscript received December 29, 2017, revised February 25, 2018; accepted April 8, 2018.

Copyright (c) 2011 IEEE. Personal use of this material is permitted. However, permission to use this material for any other purposes must be obtained from the IEEE by sending a request to pubs-permissions@ieee.org.

M. Uno is with the Faculty of Engineering, Ibaraki University, Hitachi 316-8511, Japan (e-mail: masatoshi.uno.ee@vc.ibaraki.ac.jp).

Akio Kukita is with Japan Aerospace Exploration Agency, Tsukuba, Japan (email: kukita.akio@jaxa.jp).

imbalance issues, as shown in Fig. 1. Given the tendency for considerable voltage imbalance due to the huge temperature gradient in larger systems as aforementioned, equalizers with different power capability should be used for battery- and cell-level equalizers. Equalizers capable of relatively large equalization currents are considered desirable for battery-level equalization to eliminate or preclude voltage imbalance originating from relatively large non-uniform self-discharge due to the huge temperature gradient in the battery system, as mentioned above. Meanwhile, low-power equalizers would be sufficient for cell-level equalization.

Various kinds of voltage equalization techniques have been proposed, demonstrated, and implemented to mitigate or even eliminate such voltage mismatch issues [6]. Adjacent battery-to-battery (or cell-to-cell) equalizers [see Fig. 2(a)] are the most popular equalization technique. Among these are the equalizers based on bidirectional converters, such as buck-boost converters [7]–[11] and switched capacitor converters [12]–[15]. However, since the converter count necessary in these systems are proportional to the number of batteries connected in series, these equalizers are prone to be complex and costly as the number of series connection increases. To reduce the converter count, equalizers with selection switches [see Fig. 2(b)] have been vigorously studied and developed recent years [16]–[20]. These techniques, however, require not only numerous bidirectional selection switches in proportion to the battery count but also complex equalization algorithms to properly drive selection switches depending on voltage imbalance conditions.

Meanwhile, string-to-battery (or pack-to-cell) equalizers [see Fig. 2(c)] offer reduced converter and switch counts. The most straightforward topology of the string-to-battery equalizers is a forward or flyback converter with a multi-winding transformer [21]–[23]. Although the switch count can be reduced to a few, these equalizers suffer from the design challenge of the multi-winding transformer—leakage inductances for multiple secondary windings must be strictly matched. Otherwise, voltage mismatch would remain or even be exacerbated [24], [25].

The string-to-battery equalizers based on the voltage multiplier [26]–[28] or multi-stacked buck-boost converters [29] have been proposed. In addition to the single- or two-switch topologies, these equalizers can be implemented without a multi-winding transformer, and hence offers simple circuit and ease of design, but relatively large ripple currents flow

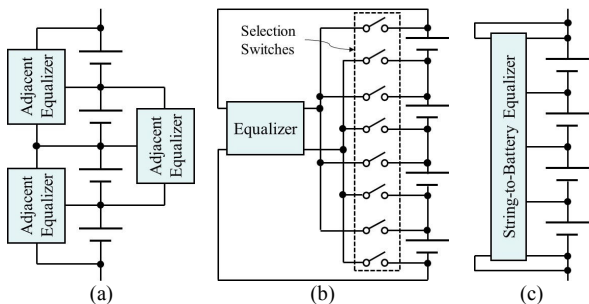


Fig. 2. Equalization architectures based on (a) adjacent battery-to-battery equalizers, (b) selection switches, and (c) string-to-battery equalizer.

through batteries. Operation modes of the equalizer base on multi-stacked buck-boost converters [29] are shown in Fig. 2 as an example. Current flowing through upper batteries are superimposed on lower ones, hence increasing ripple currents. These ripple currents tend to increase with not only equalization currents required but also the number of batteries connected in series. Therefore, smoothing capacitors with a large capacitance would be indispensable to decouple the large ripple currents. Otherwise, applications of these equalizers would be restricted to small-scale energy storage systems comprising a small number of batteries requiring small equalization currents. Given the tendency for the considerable voltage imbalance due to the huge temperature gradient in large-scale energy storage systems, equalizers capable of large equalization currents with low ripple are considered desirable for large-scale systems.

We have proposed a battery-level equalizer based on a half-bridge converter (HBC) with multi-stacked current doublers (MSCDs) in our prior study [30], and this paper presents the extended and fully developed work. The switch count of the proposed equalizer is only two, achieving the simple circuit. In addition, the proposed equalizer is capable of providing large equalization currents without increasing the ripple current. Both derivation procedure and representative topology for four batteries connected in series are presented in Section II. Detailed operation analyses under voltage-balanced and -imbalanced conditions are performed in Section III, followed by design example in Section IV. A dc equivalent circuit of the proposed equalizer is mathematically derived and verified in Section V. The experimental results of equalization tests performed for series-connected SCs and lithium-ion batteries are presented in Section VI.

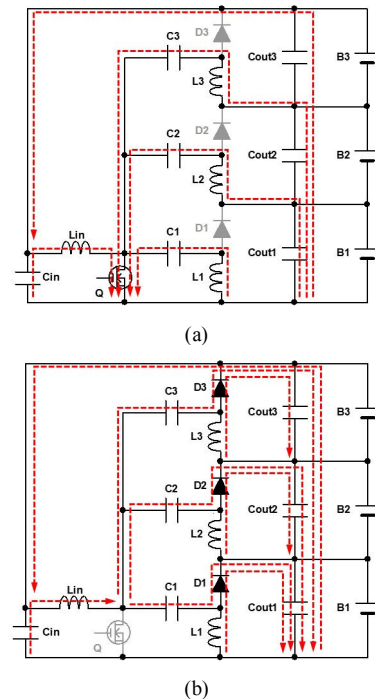


Fig. 3. Current superposition in conventional single-switch voltage equalizer in (a) on period and (b) off period.

II. PROPOSED VOLTAGE EQUALIZER USING MULTI-STACKED CURRENT DOUBLERS

A. Conventional Half-Bridge Converter with Current Doubler

A conventional HBC with a common-cathode and -anode CDs are depicted in Figs. 4(a) and (b), respectively. The secondary winding of the transformer is connected to junctions of diode-inductor pairs. Key operation waveforms in discontinuous conduction mode (DCM) are shown in Fig. 4(c). As high- and low-side switches,  $Q_a$  and  $Q_b$ , are alternately driven, the diode-inductor pairs on the secondary side operate in  $180^\circ$  out of phase, continuously supplying currents to the load. In DCM operations, both inductor currents of  $i_{L_a}$  and  $i_{L_b}$  become zero in every switching cycle (see Modes 4 and 8).

B. Circuit Description of Proposed Multi-Stacked Current Doublers

The proposed equalizer can be derived by stacking the CD circuits, as shown in Fig. 5. The proposed equalizer employs either common-cathode or -anode CDs, as illustrated in Figs. 5(a) and (b)—circuits on the primary side is not illustrated in Fig. 5(b). Smoothing capacitors connected in parallel with batteries  $B_1$ – $B_4$  are not illustrated for the sake of simplicity. For CDs to be multi-stacked, the junctions of diode-inductor pairs,  $L_{1a}$ – $D_{1a}$ – $L_{4a}$ – $D_{4a}$  and  $L_{1b}$ – $D_{1b}$ – $L_{4b}$ – $D_{4b}$ , are tied to the

transformer secondary winding through coupling capacitors of  $C_{1a}$ – $C_{4a}$  and  $C_{1b}$ – $C_{4b}$  that allow ac components only to flow through them. This means all the inductor-diode pairs are virtually driven by the same square wave voltage generated across the transformer secondary winding  $v_s$ , although they are at different dc voltage levels. The voltage equalization mechanism of the MSCD is qualitatively explained in the next subsection. Bias resistors  $R_{bias}$  are added to stabilize voltages of coupling capacitors—since  $C_{1a}$  and  $C_{1b}$  ( $i = 1 \dots 4$ ) are connected in series in the MSCDs, their voltages tend to become uncertain if without  $R_{bias}$ .

C. Voltage Equalization Mechanism

As all the CDs are ac-coupled by coupling capacitors, they can be equivalently separated and grounded as shown in Fig. 6, in which the transformer secondary winding is equivalently illustrated as a square wave generator to simplify the circuit. Obviously, all the CDs including respective batteries are connected in parallel, and therefore, all the CDs operate identically as long as the battery voltages are uniform. If battery voltages are imbalanced, currents are preferentially supplied from the secondary winding to the least charged battery having

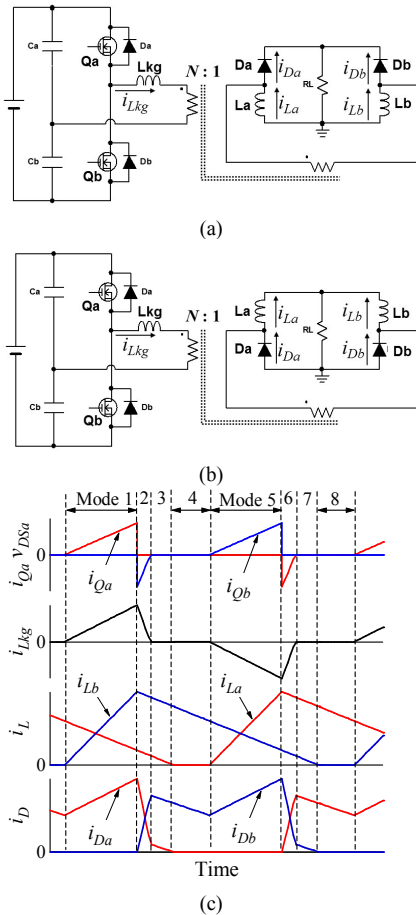


Fig. 4. (a) Common-cathode current doubler, (b) common-anode current doubler, and (c) key operation waveforms.

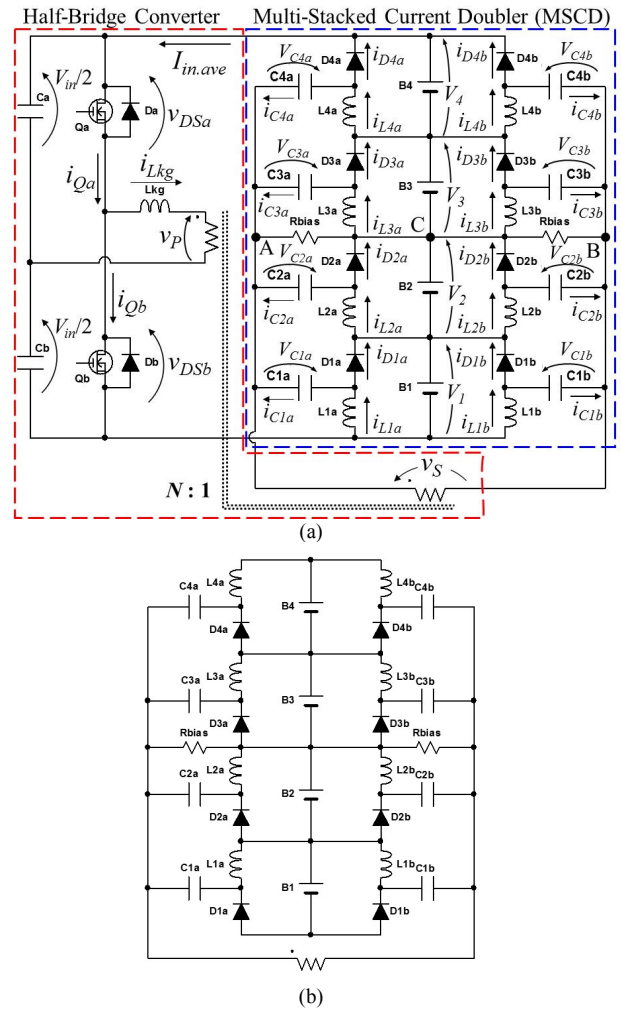


Fig. 5. Proposed two-switch voltage equalizer using a half-bridge converter with (a) common-cathode multi-stacked current doublers and (b) common-anode multi-stacked current doublers (secondary side only).

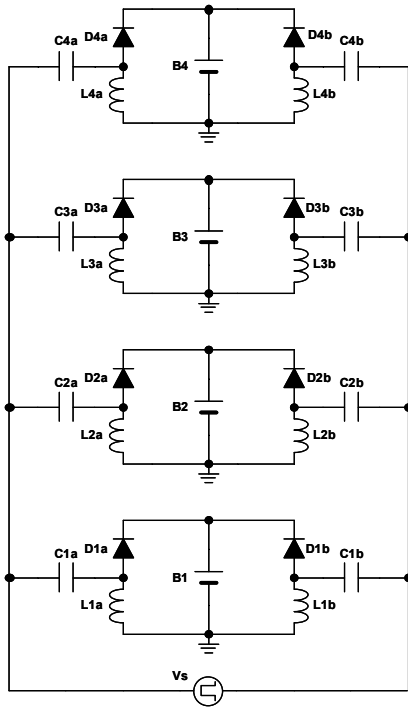


Fig. 6. Equivalent circuit of multi-stacked current doublers.

the lowest voltage in the system, eventually equalizing all the battery voltages.

The proposed equalizer is essentially a voltage equalizer that operates to unify all battery voltages. Hence, a voltage drop across an internal resistances of batteries (i.e.,  $IR$  drop) would affect the equalization performance especially when the battery string is charged/discharged with a large current. It is generally recommended to perform voltage equalization when the string's current is zero during idle periods [31] so that  $IR$  drops are negligible. Although equalization currents supplied to batteries from the voltage equalizer itself cause  $IR$  drops to some extent, the impact is considered very insignificant because an equalization current necessary in practical use is far smaller than a string's current—an equalization current as low as one-hundredth of a string current is considered sufficient to eliminate or preclude voltage imbalance [31]–[33]. In other words, even if internal resistances of batteries are mismatched due to component tolerance or uneven aging of the battery string, equalization would be appropriately performed as long as  $IR$  drops are negligibly small.

#### D. Major Features

Regardless of the number of batteries connected in series, the switch count necessary in the proposed equalizer is only two, hence significantly reducing the circuit complexity compared with conventional equalizers using individual bidirectional converters [7]–[15]. In addition to the simplified circuit, the design difficulty can also be significantly mitigated thanks to the lack of a multi-winding transformer [24], [25]. Furthermore, the proposed equalizer is capable of providing relatively large equalization currents because CDs are inherently a suitable circuit for applications needing large output currents. Hence,

the proposed voltage equalizer is more suitable for battery/module equalization rather than cell equalization, because battery voltages are more prone to be imbalanced due to the large temperature gradient in systems and require larger equalization currents, as discussed in Section I.

In DCM operations, inductor currents as well as equalization currents are automatically limited to desired current levels even at a fixed duty cycle operation without feedback control, achieving the current sensorless topology. Furthermore, since battery voltages are also automatically balanced, voltage measurement is also not necessary, allowing voltage sensors to be removed. The current and voltage sensorless equalization capability contributes to reducing the circuit complexity and cost. This is an appealing feature in comparison with equalizers using selection switches [16]–[20] and some string-to-battery equalizer [34]. These conventional topologies offer an efficient equalization by properly selecting target batteries that should receive or supply an equalization current. However, not only is individual battery voltage measurement mandatory to determine target batteries but also relatively complex equalization algorithms are necessary (especially for advanced equalization strategies, such as [20]).

#### E. Comparison with Conventional Equalizers

Component counts necessary in the proposed voltage equalizer are compared with those in conventional ones, as shown in Table I where  $n$  is the number of batteries connected in series. Adjacent equalizers [see Fig. 2(a)] require numerous switches in proportion to  $n$ , and therefore their circuit complexity tends to increase. In addition, since power transfer is limited only between adjacent two batteries, power conversion losses might collectively soar especially when  $n$  is large. Equalizers with selection switches [see Fig. 2(b)] can reduce the passive component counts and can potentially reduce circuit volume. However, in addition to the large switch count, relatively complex equalization algorithms based on individual battery voltage measurement are indispensable to perform equalization.

The reduced switch count is the most prominent feature of string-to-battery voltage equalizers [see Fig. 2(c)]. Although the topologies using a multi-winding transformer [21], [22] comprise a few passive components, the design hurdle of the transformer is cited as a top concern. A normal transformer can be employed for equalizers using a voltage multiplier [26]–[28] or multi-stacked buck-boost converters [29]. However, smoothing capacitors with a large capacitance would be necessary to decouple relatively large ripple currents, as mentioned in Section I. The equalizer based on the wave-trap concept [34] also does not need a multi-winding transformer, but the need of numerous transformers would be a major disadvantage.

The proposed voltage equalizer requires neither numerous switches nor a multi-winding transformer. The most prominent benefit is the low ripple current outputs thanks to the MSCDs, though the increased passive component counts are a disadvantage compared to conventional string-to-battery equalizers.

TABLE I  
NECESSARY COMPONENT COUNT IN PROPOSED AND CONVENTIONAL EQUALIZERS

Topology	Switch	L	C <sup>†</sup>	D	Transformer	Remarks	
Adjacent Equalizer	[7]	$n$	$n-1$	-	-	Limited power transfer only between adjacent two batteries	
	[9]	$2(n-1)$	$n-1$	-	-		
	[10]	$2(n-1)$	$2(n-1)$	$n-1$	-		
	[12]	$2n$	-	$2n-3$	-		
	[14]	$2n$	-	$n-1$	-		
Selection Switches	[17]	2 and $2n$ SSRs	-	-	2	Complex algorithm based on voltage measurement	
	[18]	$2(n+1)$	-	-	$2n-1$		1
String-to-Battery	[21]	2	-	-	$n+2$	Design hurdle of multi-winding transformer	
	[22]	2	1	2	$4n$		$1^{\dagger\dagger}$
	[34]	2	1	$n+2$	$n$	$n$	Numerous transformers
	[26]	2	-	$n+1$	$2n$	1	Large smoothing capacitors necessary to decouple large ripple currents
	[27]	2	1	$n+2$	$2n$	1	
	[28]	1	-	$n+1$	$2n$	1	
	[29]	1	$n+1$	$n$	$n$	-	
Proposed	2	$2n$	$2(n+1)$	$2n$	1	Low ripple current	

SSR(Solid State Relay)      † Smoothing capacitor is excluded  
 †† Multi-winding transformer

### III. OPERATION ANALYSIS

Equalizers must operate so that no excessive equalization current flows toward batteries. Although equalization currents can be controlled by measuring individual battery voltages and currents, numerous voltage and current sensors in proportion to the battery count would be necessary, impairing the simplicity of the proposed equalizer. To limit equalization currents within desired levels without any current and voltage sensors, operations in DCM are considered in this paper.

In general, batteries can be regarded as a constant voltage source because their dynamic responses are far slower than those of switching converters. In addition, the proposed voltage equalizer operates with a fixed duty cycle without feedback control, as discussed in Section II-D. Hence, this section focuses only on the steady-state analysis. The operation analysis in this section is performed on the premise that all circuit elements are ideal, the leakage inductance is reflected on the secondary winding in the form of  $L_{kg}' (= L_{kg}/N^2$  where  $N$  is the transformer turns ratio), and the input voltage  $V_{in} (= V_1 + V_2 + V_3 + V_4)$  is equally divided by the HBC so that voltages of  $C_a$  and  $C_b$  are  $V_{in}/2$ , as designated in Fig. 5(a). Bias resistors  $R_{bias}$  and smoothing capacitors are not illustrated in Fig. 8 for the sake of clarity.

#### A. Operation Principle

The theoretical key operation waveforms and current flow directions when the voltage of  $B_1$ ,  $V_1$ , is the lowest are shown in Figs. 7 and 8, respectively. Since Modes 1–4 and 5–8 are symmetric, operations in Modes 5–8 are not discussed to save page length. In the proposed equalizer, equalization currents preferentially flow toward the least charged battery having the lowest voltage, as mentioned in Section II-C. An equalization current supplied to  $B_i$  ( $i = 1 \dots 4$ ) is equal to the sum of the average diode currents of  $I_{Dia} + I_{Dib}$ , and also equals to the sum of the average inductor currents of  $I_{Lia} + I_{Lib}$  because an average current of a coupling capacitor in the MSCDs must be zero:

$$\begin{cases} I_{Dia} = I_{Lia} \\ I_{Dib} = I_{Lib} \end{cases} \quad (1)$$

Since no equalization current flows toward batteries with higher voltages (i.e.,  $B_2$ – $B_4$ ), the current of diodes connected to them is essentially zero, meaning these diodes do not conduct. Equation (1) suggests that the average currents of inductors for batteries with higher voltages are also zero, though ripple currents remain as shown in Fig. 7.

Average voltages of inductors and transformer windings are zero under steady-state conditions. Since the structure of the MSCDs is symmetric, voltages of  $C_{ia}$  and  $C_{ib}$ ,  $V_{Cia}$  and  $V_{Cib}$ , are essentially identical. Thanks to  $R_{bias}$ , voltages at nodes A and B are equal to that of node C [see Fig.5(a)], and therefore,

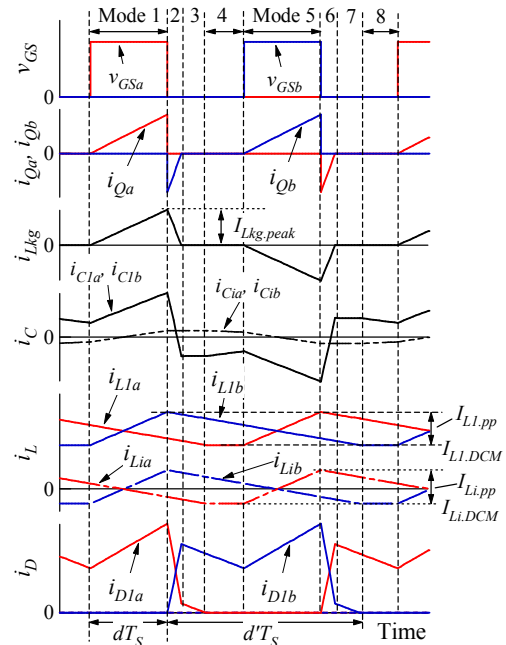


Fig. 7. Key operation waveforms under voltage-imbalanced condition ( $V_1$  is the lowest).

$$\begin{cases} V_{C1a} = V_{C1b} = -(V_1 + V_2) \\ V_{C2a} = V_{C2b} = -V_2 \\ V_{C3a} = V_{C3b} = 0 \\ V_{C4a} = V_{C4b} = V_3 \end{cases} \quad (2)$$

**Mode 1** [Fig. 8(a)]: As the high-side switch  $Q_a$  is turned on,  $V_{in}/2N$  appears across the secondary winding ( $N$  being the transformer turns ratio). The diode  $D_{1a}$ , which is connected to the least charged battery  $B_1$ , conducts while other diodes are off. Applied voltages across  $L_{1a}$  and  $L_{1b}$ ,  $v_{L1a}$  and  $v_{L1b}$ , are expressed as

$$\begin{cases} v_{L1a} = -(V_1 + V_F) \\ v_{L1b} = \left\{ \frac{V_{in}}{2N} - (V_1 + V_F) \right\} \frac{L_1}{L_1 + L_{kg}} \end{cases} \quad (3)$$

where  $V_F$  is the forward voltage drop of diodes in the MSCDs. Accordingly, currents of  $L_{1b}$ - $L_{4b}$ ,  $i_{L1b}$ - $i_{L4b}$ , start linearly increasing, while others  $i_{L1a}$ - $i_{L4a}$  decrease. Meanwhile, currents on the primary side,  $i_{Qa}$  and  $i_{Lkg}$ , also start linearly increasing from zero, and  $i_{Qa}$  and  $i_{Lkg}$  peak at the end of Mode 1.

**Mode 2** [Fig. 8(b)]: This mode begins as  $Q_a$  is turned off. The anti-parallel diode  $D_b$  conducts, and  $i_{Lkg}$  decreases. Both of  $D_{1a}$  and  $D_{1b}$  conduct in the MSCDs, and therefore, inductor voltages in this mode are

$$\begin{cases} v_{L1a} = -(V_1 + V_F) \\ v_{L1b} = -(V_1 + V_F) \end{cases} \quad (4)$$

Hence,  $i_{L1a}$  and  $i_{L1b}$  decrease and flow toward  $B_1$  through  $D_{1a}$  and  $D_{1b}$ , respectively, whereas other diodes are off. This mode lasts until  $i_{Lkg}$  reaches zero.

**Mode 3** [Fig. 8(c)]: No current flows in the HBC on the primary side, while both  $D_{1a}$  and  $D_{1b}$  are still conducting (i.e., the operation on the secondary side are nearly identical to those in Mode 2). This mode ends when  $i_{D1a}$  reaches zero.

**Mode 4** [Fig. 8(d)]: This mode begins as  $i_{D1a}$  reaches zero.  $v_{L1a}$  is zero in this mode, and hence, its current  $i_{L1a}$  is essentially constant. Meanwhile,  $v_{L1b}$  is same as that in Modes 2 and 3, and therefore  $i_{L1b}$  still linearly decreases;

$$\begin{cases} v_{L1a} = 0 \\ v_{L1b} = -(V_1 + V_F) \end{cases} \quad (5)$$

As the lower switch  $Q_b$  is turned on, the next mode, Mode 5, begins. Operations in Modes 5-8 are symmetric to Modes 1-4 and can be explained similarly.

As can be seen in Fig. 8, currents from the equalizer flow toward only  $B_1$ , the least charged battery with the lowest voltage. In addition, currents from the two inductors (i.e.,  $i_{L1a}$  and  $i_{L1b}$ ) are 180° out of phase and supplied to  $B_1$  in an interleaving manner by the MSCDs, doubling the substantial switching frequency and reducing the ripple current. The proposed equalizer is thus considered suitable to provide relatively large equalization currents, and the required capacitance for smoothing capacitors can be reduced compared with those in conventional equalizer [29].

In the proposed equalizer, ripple currents flow through all inductors and capacitors that are connected in parallel with not only  $B_1$  but also  $B_2$ - $B_4$  (see Figs. 7 and 8), hence unavoidably generating Joule losses to some extent. Although minor, these

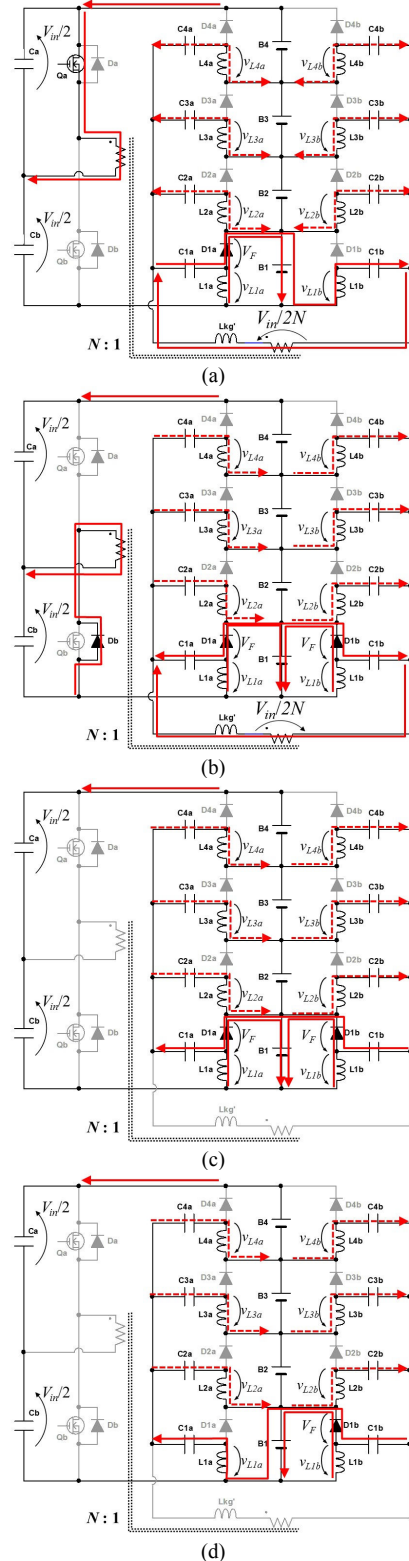


Fig. 8. Operation modes when  $B_1$  is the least charged battery: (a) Mode 1, (b) Mode 2, (c) Mode 3, (d) Mode 4.

Joule losses lead to waste of stored energies in batteries. However, since power processed in equalizers is generally lower than one-hundredth of strings' power, the minor losses due to the ripple currents would have a trivial impact on a systems' efficiency [31]-[33].

### B. DCM Operation Criterion

Based on the volt-second balance on  $L_{1a}$  and  $L_{1b}$ , the duty cycle of diodes,  $d'$  (designated in Fig. 7), can be yielded from (3)–(5) as

$$\left\{ \frac{V_{in}}{2N} - (V_1 + V_F) \right\} \frac{L_1}{L_1 + L_{kg}'} d - (V_1 + V_F) d' = 0, \quad (6)$$

$$\Rightarrow d' = \frac{V_{in} - 2N(V_1 + V_F)}{2N(V_1 + V_F)} \frac{L_1}{L_1 + L_{kg}'},$$

where  $d$  is the duty cycle of each switch. For the equalizer to operate in DCM,  $d' < (1 - d)$  must be ensured, whereupon the critical duty cycle  $d_{critical}$  can be obtained as

$$d_{critical} < \frac{2N(V_1 + V_F)(L_1 + L_{kg}')}{V_{in}L - 2N(V_1 + V_F)L_{kg}'} \approx \frac{2N(V_1 + V_F)}{V_{in}}. \quad (7)$$

### C. Currents under Voltage-Imbalanced Condition

The peak-to-peak currents of  $i_{Lix}$  ( $i = 1 \dots 4$ ,  $x = a$  or  $b$ ),  $I_{Lix,pp}$ , as designated in Fig. 7, are given by

$$I_{Lix,pp} = \left\{ \frac{V_{in}}{2N} - (V_1 + V_F) \right\} \frac{dT_S}{L_{ix} + L_{kg}'}, \quad (8)$$

where  $T_S$  is the switching period, and  $L_{ix}$  is the inductance of  $L_{1a}$ – $L_{4a}$  and  $L_{1b}$ – $L_{4b}$ . The average currents of  $L_{ix}$  are expressed as

$$\begin{cases} I_{Lix} = \frac{I_{Lix,pp}(d + d')}{2} + I_{Lix,DCM} \\ I_{Lix} = \frac{I_{Lix,pp}(d + d')}{2} + I_{Lix,DCM} = 0 \quad (i = 2 \dots 4) \end{cases}, \quad (9)$$

where  $I_{Lix,DCM}$  is the inductor current during Modes 4 or 8. From the current flow paths shown in Fig. 8(d),

$$I_{Lix,DCM} + \sum_{i=2}^4 I_{Lix,DCM} = 0. \quad (10)$$

From (8)–(10),

$$I_{Lix} = \frac{d + d'}{2} \sum_{i=1}^4 I_{Lix,pp} = \sum_{i=1}^4 \left\{ \frac{V_{in}}{2N} - (V_1 + V_F) \right\} \frac{d(d + d')T_S}{2(L_{ix} + L_{kg}')}. \quad (11)$$

By assuming all inductances are uniform as  $L$ , (11) can be rewritten as

$$I_{Lix} = \left\{ \frac{V_{in}}{2N} - (V_1 + V_F) \right\} \frac{2d(d + d')T_S}{L + L_{kg}'}. \quad (12)$$

The equalization current supplied to  $B_i$  is equal to the sum of average diode currents of  $I_{Dia} + I_{Dib}$  or  $I_{Lia} + I_{Lib}$ , as expressed by (1). Provided that the variation ranges of  $V_{in}$  and  $V_1$  are known, (12) indicates that the equalization current supplied to  $B_1$  can be limited to a desired current level, even at a fixed  $d$  without feedback control.

The peak current of the transformer primary winding,  $I_{Lkg,peak}$ , is expressed as

$$I_{Lkg,peak} = \frac{3(I_{Lix,pp} + I_{Lix,DCM}) + (I_{Lix,pp} + I_{Lix,DCM})}{N} = \sum_{i=1}^4 \left\{ \frac{V_{in}}{2N} - (V_1 + V_F) \right\} \frac{dT_S}{N(L_{ix} + L_{kg}')}. \quad (13)$$

By assuming all inductances are matched as  $L$ , (13) can be simplified to be

$$I_{Lkg,peak} = \left\{ \frac{V_{in}}{2N} - (V_1 + V_F) \right\} \frac{4dT_S}{N(L + L_{kg}')}. \quad (14)$$

The length of Mode 2,  $T_2$ , is

$$T_2 = \frac{V_{in} - 2N(V_1 + V_F)}{V_{in}} \frac{L_{kg}'}{L_i + L_{kg}'} 4dT_S. \quad (15)$$

The average input current of the equalizer,  $I_{in,ave}$ , is obtained from (14) and (15). Since  $T_2$  is rather shorter than  $dT_S$  in practical operations,  $I_{in,ave}$  can be approximated to be

$$I_{in,ave} = \frac{I_{Lkg,peak}(dT_S + T_2)}{2T_S} \approx \left\{ \frac{V_{in}}{2N} - (V_1 + V_F) \right\} \frac{2d^2T_S}{N(L_i + L_{kg}')}. \quad (16)$$

Similar to (12),  $I_{in,ave}$  can be limited to a desired current level, even at a fixed  $d$  as long as the variation ranges of  $V_{in}$  and  $V_1$  are known.

### D. Currents under Voltage-Balanced Condition

In this subsection, currents under a voltage-balanced condition are yielded and compared with those under the voltage-imbalanced condition discussed in the previous subsection. The equalized voltage is defined as  $V_e = V_1 \dots V_4$ . Under a voltage-balanced condition, both equations in (9) can be expressed in the identical form as

$$I_{Lix} = \frac{I_{Lix,pp}(d + d')}{2} + I_{Lix,DCM}. \quad (17)$$

From (8), (10), and (17),

$$I_{Lix} = \sum_{i=1}^4 \left\{ \frac{V_{in}}{2N} - (V_e + V_F) \right\} \frac{d(d + d')T_S}{2(L_i + L_{kg}')} - \sum_{i=2}^4 I_{Lix}. \quad (18)$$

This equation implies that average inductor currents are interdependent. If all average inductor currents are equal to  $I_{L1x} \dots I_{L4x} = I_{Lx}$  and inductances are uniform as  $L$ , (18) can be simplified to

$$I_{Lx} = \left\{ \frac{V_{in}}{2N} - (V_e + V_F) \right\} \frac{d(d + d')T_S}{2(L + L_{kg}')}. \quad (19)$$

Comparing (12) and (19),  $I_{Lx}$  under the voltage-balanced condition is quarter of that under the voltage-imbalanced condition. In other words, the sum of  $I_{L1} \dots I_{L4}$  is identical regardless of whether battery voltages are balanced or imbalanced.

As (14) implies,  $I_{Lkg,peak}$  is dependent on the voltage of the least charged battery and is independent on whether voltages are balanced, meaning the average input current  $I_{in,ave}$  under a voltage-balanced condition is identical to that under voltage-imbalanced conditions, as expressed by (16).

### E. Impact of Component Tolerance

The MSCDs consist of passive components only, meaning component tolerance might adversely affect equalization performance. The equivalent circuit shown in Fig. 4 suggested that all battery voltages can be automatically equalized with the proposed equalizer. However, as indicated by (7), a battery voltage [ $V_1$  in the case of (7)] depends on  $V_F$ , and therefore, the mismatch in  $V_F$  would eventually lead to non-uniform battery voltages. However, if a battery voltage exceeds  $V_F$  to a sufficient extent, the impact of this mismatch would be negligibly small. In general, since voltages of batteries comprising several cells connected in series are adequately higher than  $V_F$ , the mismatch in  $V_F$  does not have a significant

impact. For instance,  $\pm 10\%$  tolerance of Schottky diode with  $V_F = 0.5$  V would lead to  $\pm 50$  mV imbalance, and it corresponds to merely  $\pm 0.33\%$  voltage imbalance for batteries with 15 V.

The mismatch in capacitance of coupling capacitors also has no significant impact on equalization performance because their voltages under a steady-state condition can be considered constant regardless of capacitance mismatch, provided their capacitances are sufficient.

Inductance mismatch would result in non-uniform inductor currents, as indicated by (11); average inductor currents are dependent on inductances. The average inductor currents under the voltage-imbalance condition are four times greater than those under the voltage-balanced condition as discussed in Sections III-C and -D, and therefore, inductors experience the largest current stress under the voltage-imbalance condition. However, since inductor currents are limited to a desired current level as long as the DCM operation is ensured, inductance mismatch does not result in a serious current mismatch. Furthermore, regardless of any mismatch in inductances and/or inductor currents, all battery voltages can be eventually equalized as (7) indicates—a battery voltage is independent on inductances if  $L_{kg}' \ll L$ .

#### IV. DESIGN EXAMPLE

In general, equalizers with a power capability of one-hundredth of a string power are considered sufficient to equalize battery voltages [31]–[33]. In this section, as an example, an 80-W prototype of the proposed equalizer for four batteries connected in series is designed for the target below:

- The maximum input voltage  $V_{in}$  is 70.0 V ( $V_1$ – $V_4$  are equalized as  $V_e = 17.5$  V) under the voltage balanced condition
- Voltage imbalance in the worst case is that one of four battery voltages is  $0.8V_e$  while others are  $V_e$  (i.e.,  $V_{in} = 3.8V_e$ )
- Duty cycle  $d$  is fixed to be 0.35
- Switching frequency is 200 kHz ( $T_S = 5.0$   $\mu$ s)

1)  $d$  is fixed, whereas  $d'$  is dependent on the lowest battery voltage (i.e.,  $0.8V_e$ ) according to (6). To ensure the DCM operation even in the worst imbalance case, in which  $d'$  becomes the largest, the transformer turns ratio  $N$  should be properly determined so that  $d' \leq 0.65$ . Assuming  $V_F$  and  $L_{kg}'$  are negligibly small compared to  $V_e$  and  $L_i$ , respectively,  $N$  can be determined from (6), as

$$0.65 = \frac{3.8V_e - 2N \times 0.8V_e}{2N \times 0.8V_e} \cdot 0.35 \Rightarrow N = 0.831 \cdot \quad (20)$$

$N$  was approximated to be 0.8 ( $N_1:N_2 = 12:15$  for a prototype).

2) Assuming the power conversion efficiency is 90%, the average input current,  $I_{in,ave}$ , is

$$I_{in,ave} = \frac{80\text{ W}}{0.9 \times 70\text{ V}} \approx 1.27\text{ A} \cdot \quad (21)$$

From (16), the inductance  $L_i$  is determined as

$$L_i = \left( \frac{V_{in} - V_i}{2N} \right) \frac{2d^2 T_S}{I_{in,ave} N} = 31.7\ \mu\text{H} \approx 33\ \mu\text{H} \cdot \quad (22)$$

3) According to (12), the maximum average inductor current

is around 3.0 A at  $V_{in} = 70.0$  V. A mathematical expression for a current of capacitor  $C_{ix}$ ,  $i_{Cix}$ , is quite complex but  $i_{Cix} \leq \max\{I_{Lia}, I_{Lib}\}$  can be assumed according to the waveforms and current flow directions shown in Figs. 7 and 8. Based on this assumption, the amount of charge transferred can be approximated as

$$Q < 0.5 I_{Lix} T_S = 7.5\ \mu\text{C} \cdot \quad (23)$$

In this design example, the capacitance of  $C_{ix}$  is determined so that its ripple voltage  $V_{ripple}$  is below 0.5% of its steady-state voltage. The largest steady-state voltage of capacitors is 35 V ( $= V_{C1a} = V_{C2a}$ ) according to (2). Hence, the capacitance  $C_{ix}$  is determined as

$$C_{ix} = \frac{Q}{V_{ripple}} = \frac{7.5\ \mu\text{C}}{0.5\% \times 35\text{ V}} = 42.9\ \mu\text{F} \approx 47\ \mu\text{F} \cdot \quad (24)$$

#### V. SIMULATION-BASED EQUALIZATION

##### A. Circuit Description

By expressing inductors as constant current sources, the dc equivalent circuit of the proposed voltage equalizer can be derived, as shown in Fig. 9. Each inductor current  $I_{Lix}$  in the MSCDs is programmed to obey (19), while the input current  $I_{in}$  is equal to  $I_{in,ave}$  (16). As (12) and (19) indicate,  $I_{Lix}$  concentrates to the least charged battery under voltage-imbalance conditions, whereas it flows toward respective battery when battery voltages are balanced. In order to emulate such behavior, current sources  $I_{L1a}$ – $I_{L4a}$  and  $I_{L1b}$ – $I_{L4b}$  are connected in parallel through an ideal multi-winding transformer—the introduction of the ideal multi-winding transformer allows batteries to be connected in series while current sources  $I_{L1a}$ – $I_{L4a}$  and  $I_{L1b}$ – $I_{L4b}$  to be virtually connected in parallel.

The derived dc equivalent circuit is a very useful tool to quickly investigate equalization behaviors in simulation analyses because it contains no high-frequency switching devices. In general, voltage equalizers operate at frequencies higher than several ten kHz, while equalization processes take minutes to hours or even days for large-scale systems. In other words, to investigate equalization behaviors with the original

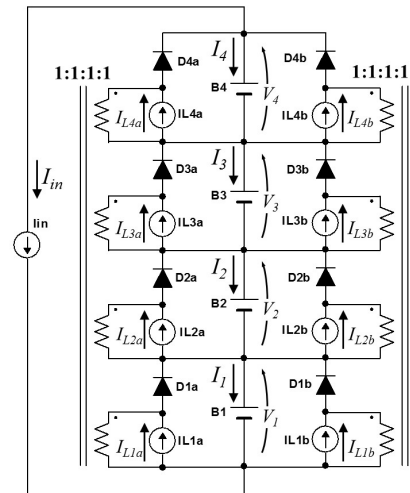


Fig. 9. DC equivalent circuit of the proposed equalizer.

circuit shown in Fig. 5, simulation analyses at high frequency need to be performed for a long stretch of time, impractically increasing simulation burden and time. With the derived dc equivalent circuit, on the other hand, simulation analyses can be completed in an instance, thus allowing designers to quickly grasp equalization behaviors.

*B. Equalization Test*

Simulation-based equalization tests were performed using the original and dc equivalent circuits, shown in Figs. 5 and 9, respectively. Component values for the experimental prototype (see Table II) were applied to the simulation analysis. Capacitors with a 100 mF capacitance and 100 mΩ equivalent series resistance (ESR) were used as batteries.

Resultant equalization profiles of the original and dc equivalent circuits are shown and compared in Fig. 10(a). At the beginning of the test,  $V_1$  was the lowest and increased as the equalization current was supplied to B<sub>1</sub> in the form of  $I_{L1a} + I_{L1b}$ , and the current of B<sub>1</sub>,  $I_1$ , was positive as  $I_1 = (I_{L1a} + I_{L1b}) - I_{in}$ .

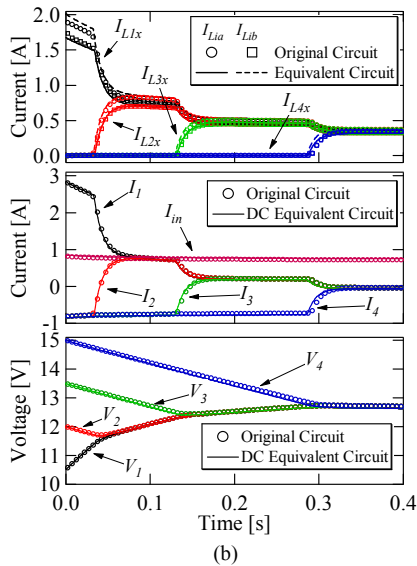
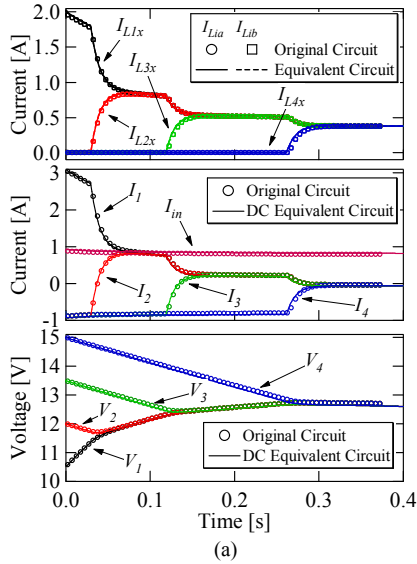


Fig. 10. Simulation equalization profiles of original and dc equivalent circuits with (a) matched inductance and (b) mismatched inductances.

$I_2$ – $I_4$ , on the other hand, were negative because B<sub>2</sub>–B<sub>4</sub> provided  $I_{in}$  to the equalizer without receiving equalization currents. As  $V_1$  caught up with  $V_2$ ,  $I_2$  became positive because not only  $V_1$  but also  $V_2$  were the lowest at this moment.  $V_1$  and  $V_2$  started to increase at the same rate, while  $V_3$  and  $V_4$  kept declining as  $I_3$  and  $I_4$  were negative, meaning B<sub>3</sub> and B<sub>4</sub> supplied  $I_{in}$ . On the basis of this energy redistribution manner, all the battery voltages were balanced 0.3 s after the start of the simulation. Overall, the equalization profiles of the original and dc equivalent circuits were in good agreement, verifying the inductor current model as well as the derived dc equivalent circuit.

To investigate the impact of component tolerance, similar equalization test was performed with the extremely-mismatched inductance condition.  $L_{1b}$  was mismatched to be 100 μH while others were unchanged from 33 μH. The equalization profiles are shown in Fig. 10(b).  $I_{L1a}$  and  $I_{L1b}$  were imbalanced due to the inductance mismatch. Since the average inductor currents are interdependent as (18), other inductor currents were also slightly imbalanced. Despite the inductor current mismatch, all battery voltages were eventually unified, similar to the result under the inductance-matched conditions [see Fig. 10(a)]. The original and derived dc equivalent circuits showed good agreement even under the inductance-mismatched condition, verifying the derived dc equivalent circuit.

VI. EXPERIMENTAL RESULTS

*A. Prototype and Experimental Conditions*

An 80-W prototype for four batteries connected in series was built, as shown in Fig. 11. Component values are listed in Table II. The prototype was operated at a switching frequency of 200 kHz with  $d = 0.35$  to ensure DCM operations.

The experimental setup to measure power conversion

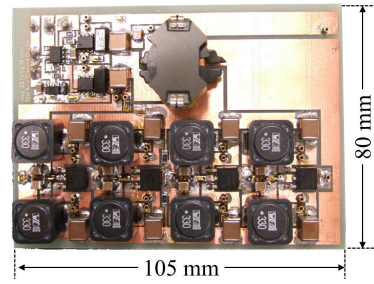


Fig. 11. A photograph of 80-W prototype for four batteries connected in series.

TABLE II  
CIRCUIT ELEMENT LIST

Element	Value
$C_{1a}$ – $C_{4a}$ , $C_{1b}$ – $C_{4b}$	Ceramic Capacitor, 47 μF
$C_{out1}$ – $C_{out4}$	Ceramic Capacitor, 44 μF
$D_{1a}$ – $D_{4a}$ , $D_{1b}$ – $D_{4b}$	Schottky Diode, 12CWQ04FN, $V_F = 0.48$ V
$L_{1a}$ – $L_{4a}$ , $L_{1b}$ – $L_{4b}$	33 μH
Transformer	$N_1:N_2 = 12:15$ , $L_{kg} = 0.3$ μH, $L_{mg} = 505$ μH
$Q_a$ , $Q_b$	FDS86240, $R_{on} = 35.3$ mΩ
$D_a$ , $D_b$	Schottky Diode, D3FJ10, $V_F = 0.74$ V
$C_a$ , $C_b$	Ceramic Capacitor, 20 μF

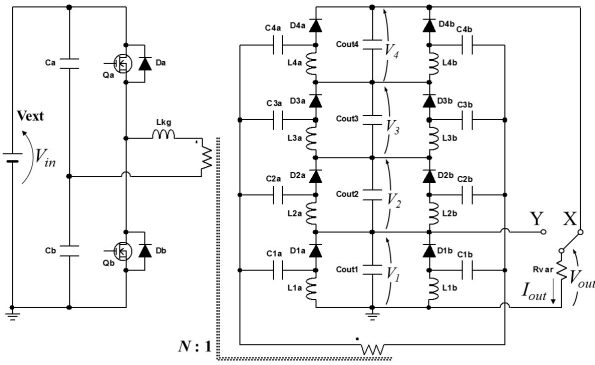
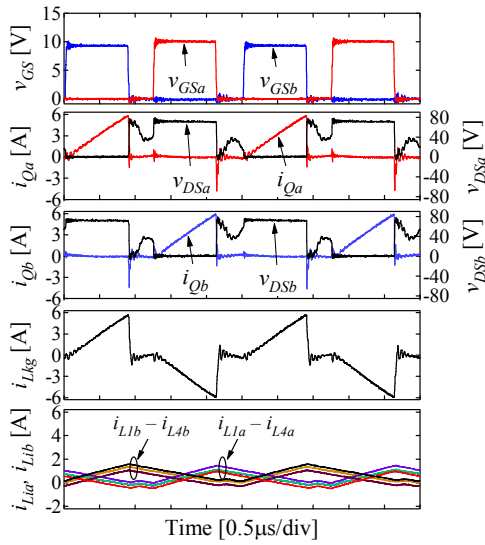
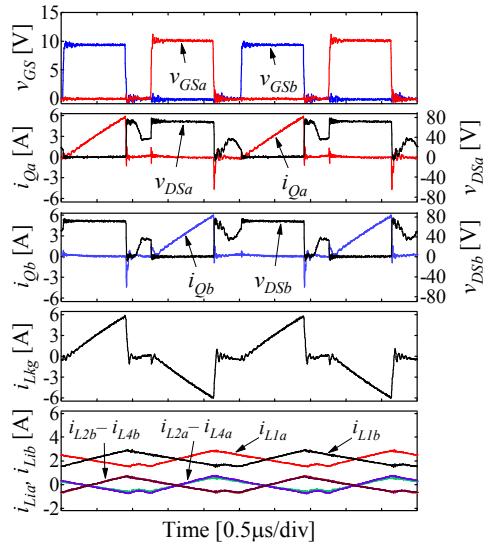


Fig. 12. Experimental setup for efficiency measurement.



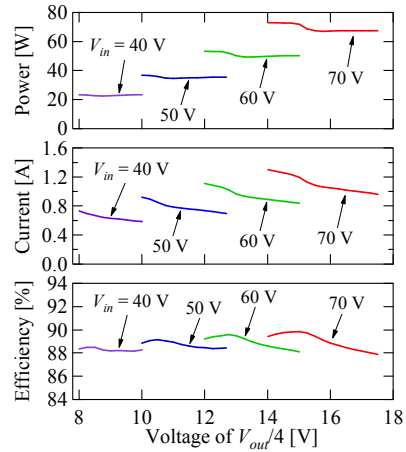
(a)



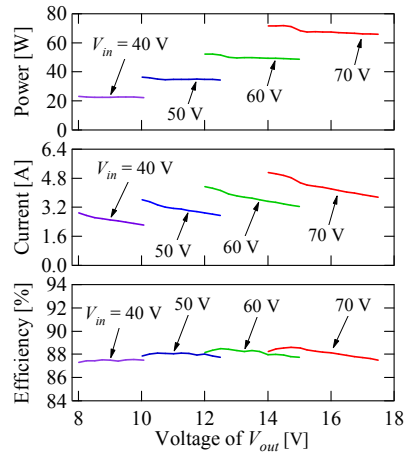
(b)

Fig. 13. Measured key waveforms under (a) voltage-balanced and (b) voltage-imbalanced conditions at  $V_{in} = 70$  V and  $V_l = 15$  V.

efficiencies and key operation waveforms are shown in Fig. 12. The input and output of the equalizer were separated, while an external power supply  $V_{ext}$  was used to power the equalizer. All batteries were removed, and smoothing capacitors  $C_{out1}-C_{out4}$



(a)



(b)

Fig. 14. Measured power conversion efficiencies and output characteristics under (a) voltage-balanced and (b) voltage-imbalanced conditions.

alone sustained the voltages of  $V_1-V_4$ . A variable resistor  $R_{var}$  was connected to the MSCDs via the selectable intermediate tap to emulate voltage-balanced and -imbalanced conditions. With the tap X selected, the current flows under the voltage-balanced condition can be emulated because all the CDs uniformly supply currents to  $R_{var}$ . Meanwhile, when tap Y is selected, the current is drawn from only the CD corresponding to the lowest position, emulating the current flows under the voltage-imbalanced condition shown in Fig. 8.

### B. Fundamental Performance

The measured key waveforms at  $V_{in} = 70$  V and  $V_l = 15$  V under voltage-balanced and -imbalanced conditions are shown in Figs. 13(a) and (b), respectively. Under the voltage-balanced condition shown in Fig. 13(a),  $i_{L1a}-i_{L4a}$  and  $i_{L1b}-i_{L4b}$  were slightly imbalanced probably due to minor inductance mismatch, as discussed in Section III-D and implied by (18). Under the voltage-imbalanced condition shown in Fig. 13(b), on the other hand, the mismatches between  $i_{L1a}-i_{L4a}$  and  $i_{L1b}-i_{L4b}$  were very minor. Average currents of  $i_{L1a}$  and  $i_{L1b}$  were substantial, whereas those of others were zero, and hence,  $B_1$  only received the equalization current. Meanwhile, the

measured waveforms related to the HBC under voltage-balanced and -imbalanced conditions were nearly identical, verifying that the operation of the HBC was unaffected by whether voltages are balanced or not, as mentioned in Section III-D.

The measured power conversion efficiencies and output characteristics under voltage-balanced and -imbalance conditions are shown in Figs. 14(a) and (b), respectively. Measured output powers were almost independent of whether the voltages were balanced, as tendencies of output powers in Figs. 14(a) and (b) were nearly identical. Output currents under the voltage-imbalanced condition were four times greater than those under voltage-balanced condition because the current from the secondary winding concentrated to the CD placed at the lowest position. Meanwhile, measured efficiencies under the voltage-imbalanced condition were somewhat inferior to those under the voltage-balanced condition. The lower efficiencies under the voltage-imbalanced condition were attributable to the increased Joule loss due to the current concentration. The currents in the MSCDs under the voltage-balanced condition uniformly flow through respective CDs, whereas those under the voltage-imbalanced condition mainly flowed in the CD at the lowest position, hence increasing the Joule losses.

*C. Equalization for Series-Connected Supercapacitors and Lithium-Ion Batteries*

Series-connected SC modules, each with a capacitance of 220 F at a rated charge voltage of 15 V, were used for the experimental equalization. The initial voltages of SCs were intentionally imbalanced between approximately 10 and 15 V, and the equalization was performed from an initially-voltage-imbalanced condition—module voltages were unrealistically imbalanced in order to verify the equalization performance of the proposed equalizer and to emphasize experimental results.

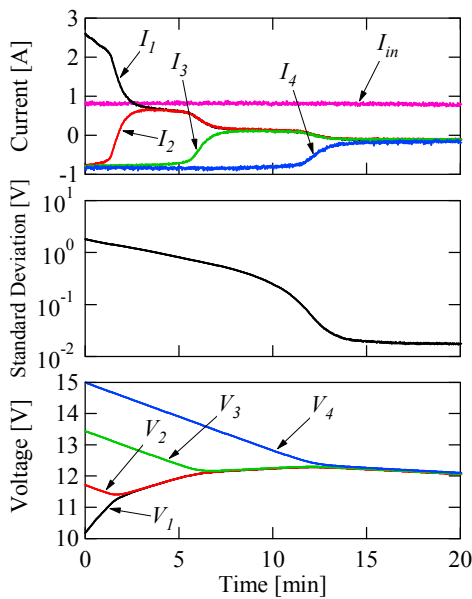


Fig. 15. Experimental equalization profiles of four supercapacitor modules connected in series.

The currents of SC modules  $I_1$ – $I_4$  and the input current of the equalizer  $I_{in}$  were also measured.

The resultant equalization profiles are shown in Fig. 15. At the beginning of the experiment,  $B_1$  only received the positive (or charging) current of  $I_1$ , and  $V_1$  increased. Meanwhile, other modules supplied the input current of  $I_{in}$  for the equalizer’s input, hence  $I_2$ – $I_4$  were negative (or discharging) and  $V_2$ – $V_4$  decreased. As  $V_1$  caught up with  $V_2$ ,  $I_2$  gradually changed from negative to positive because both  $B_1$  and  $B_2$  were the least charged modules at this moment.  $B_3$  and  $B_4$ , on the other hand, continued to supply  $I_{in}$  for the equalizer, and  $V_3$  and  $V_4$  still declined. The energies of modules with higher initial voltages were therefore redistributed to those with lower initial voltages via the equalizer. The voltage imbalance was gradually eliminated, and all the module voltages eventually became uniform. The standard deviation of module voltages at the end of the experiment was as low as 20 mV, demonstrating the equalization performance of the proposed voltage equalizer.

The module voltages kept decreasing even after they were sufficiently equalized because the voltage equalizer was still operating. In other words, the voltage equalizer needlessly circulated the energy of modules, some of which was lost in the course of the needless energy redistribution. Therefore, the voltage equalizer should be disabled when module voltages are well balanced, and voltage equalization is no longer necessary.

Similar experimental equalization test was also performed for lithium-ion polymer batteries each with a capacity of 2500 mAh at a rated charge voltage of 16.8 V from an initially-voltage-imbalanced condition, as shown in Fig. 16. Each battery contained four cells connected in series. Although the resultant profiles were somewhat elusive due to the nonlinear voltage characteristics of lithium-ion batteries, the voltage imbalance gradually disappeared, and all the battery voltages were eventually unified in the same manner as for SC modules.

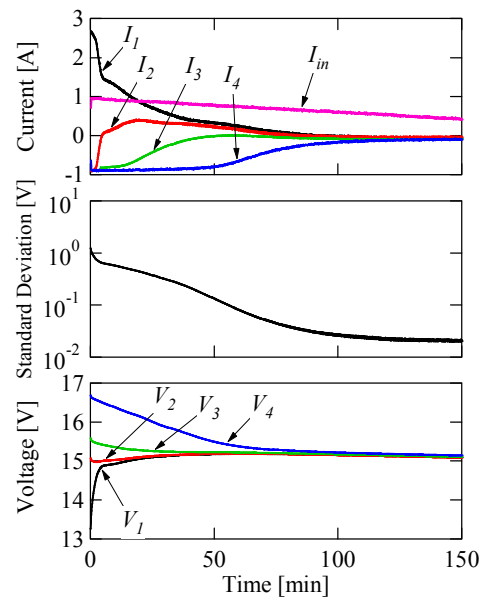


Fig. 16. Experimental equalization profiles of four lithium polymer batteries connected in series.

## VII. CONCLUSIONS

The two-switch voltage equalizer using HBC with MSCDs was proposed in this paper. Since the proposed equalizer comprises two switches without the need for a multi-winding transformer, the circuit can be simplified while eliminating the design difficulty associated with the multi-winding transformer. In addition, the proposed equalizer is capable of providing relatively large equalization currents without increasing ripple current thanks to the interleaved operation of the MSCDs.

To eliminate the feedback control loop and thus further simplify the circuitry, the proposed voltage equalizer was designed to operate in DCM, whereby currents can be automatically limited to desired levels without feedback control. Fundamental operation analysis in DCM was performed to theoretically express currents in the equalizer. The dc equivalent circuit of the proposed voltage equalizer was also derived based on the detailed operation analysis.

The 80-W prototype for four batteries connected in series was built to experimentally verify the proposed equalizer. Experimental equalization tests were performed for series-connected SC modules and lithium polymer batteries from initially-voltage-imbalanced conditions. The voltage imbalance was gradually eliminated by the equalizer, and all the voltages eventually became uniform, demonstrating the equalization performance of the proposed equalizer.

## REFERENCES

- [1] M. Zolot, A. A. Pesaran, and M. Mihalic, "Thermal evaluation of Toyota Prius battery pack," *SAE Trans.*, 2002-01-1962.
- [2] X. M. Xu, R. He, "Research on the heat dissipation performance of battery pack based on forced air cooling," *J. Power Sources*, vol. 240, pp. 33–41, Oct. 2013.
- [3] Z. Zhang, H. Gui, D.J. Gu, Y. Yang, and X. Ren, "A hierarchical active balancing architecture for lithium-ion batteries," *IEEE Trans. Power Electron.*, vol. 32, no. 4, pp. 2757–2768, Apr. 2017.
- [4] H. Chen, L. Zhang, and Y. Han, "System-theoretic analysis of a class of battery equalization systems: mathematical modeling and performance evaluation," *IEEE Trans. Veh. Technol.*, vol. 64, no. 4, pp. 1445–1457, Apr. 2015.
- [5] H. S. Park, C. H. Kim, K. B. Park, G. W. Moon, and J. H. Lee, "Design of a charge equalizer based on battery modularization," *IEEE Trans. Veh. Technol.*, vol. 58, pp. 3216–3223, Sep. 2009.
- [6] J. G. Lozano, E. R. Cadaval, M. I. M. Montero, M. A. G. Martinez, "Battery equalization active methods," *J. Power Sources*, vol. 246, pp. 934–949, Jan. 2014.
- [7] P. A. Cassani and S. S. Williamson, "Feasibility analysis of a novel cell equalizer topology for plug-in hybrid electric vehicle energy-storage systems," *IEEE Trans. Veh. Technol.*, vol. 58, no. 8, pp. 3938–3946, Oct. 2009.
- [8] T. H. Phung, A. Collet, and J. Crebier, "An optimized topology for next-to-next balancing of series-connected lithium-ion cells," *IEEE Trans. Power Electron.*, vol. 29, no. 9, pp. 4603–4613, Sep. 2014.
- [9] K. Nishijima, H. Sakamoto, and K. Harada, "A PWM controlled simple and high performance battery balancing system," in Proc. *IEEE Power Electron. Spec. Conf.*, pp. 517–520, Jun. 2000.
- [10] Y. S. Lee and M. W. Cheng, "Intelligent control battery equalization for series connected lithium-ion battery strings," *IEEE Trans. Ind. Electron.*, vol. 52, no. 5, pp. 1297–1307, Oct. 2005.
- [11] Y. S. Lee, M. W. Cheng, S. C. Yang, and C. L. Hsu, "Individual cell equalization for series connected lithium-ion batteries," *IEICE Trans. Commun.*, vol. E89-B, no. 9, pp. 2596–2607, Sep. 2006.
- [12] A. Baughman and M. Ferdowsi, "Double-tiered switched-capacitor battery charge equalization technique," *IEEE Trans. Ind. Appl.*, vol. 55, no. 6, pp. 2277–2285, Jun. 2008.
- [13] R. Lu, C. Zhu, L. Tian, and Q. Wang, "Super-capacitor stacks management system with dynamic equalization techniques," *IEEE Trans. Magnetics*, vol. 43, no. 1, pp. 254–258, Jan. 2007.
- [14] M. Uno and K. Tanaka, "Influence of high-frequency charge-discharge cycling induced by cell voltage equalizers on the life performance of lithium-ion cells," *IEEE Trans. Veh. Technol.*, vol. 60, no. 4, pp. 1505–1515, May 2011.
- [15] M. Uno and H. Toyota, "Equalization technique utilizing series-parallel connected supercapacitors for energy storage system," in Proc. *IEEE Int. Conf. Sustainable Energy*, pp. 999–1003, Nov. 2008.
- [16] C. H. Kim, M. Y. Kim, H. S. Park, and G. W. Moon, "A modularized two-stage charge equalizer with cell selection switches for series-connected lithium-ion battery string in a HEV," *IEEE Trans. Power Electron.*, vol. 27, no. 8, pp. 3764–3774, Aug. 2012.
- [17] C. H. Kim, M. Y. Kim, and G. W. Moon, "A modularized charge equalizer using a battery monitoring IC for series-connected Li-ion battery strings in electric vehicles," *IEEE Trans. Power Electron.*, vol. 28, no. 8, pp. 3779–3787, Aug. 2013.
- [18] A. M. Imtiaz, F. H. Khan, and H. Kamath, "Time shared flyback converter based regenerative cell balancing technique for series connected Li-ion battery strings," *IEEE Trans. Power Electron.*, vol. 28, no. 12, pp. 5960–5975, Dec. 2013.
- [19] M. M. Hoque, M. A. Hannan, and A. Mohamed, "Voltage equalization control algorithm for monitoring and balancing of series connected lithium-ion battery," *J. Renewable and Sustainable Energy*, vol. 8, pp. 025703, Mar. 2016.
- [20] Z. Shen, H. Gui, and L.M. Tolbert, "A battery cell balancing control scheme with minimum charge transfer," in Proc. *IEEE Energy Conversion Cong. Expo. (ECCE)*, pp. 1–6, Sep. 2016.
- [21] N. H. Kutkut, D. M. Divan, and D. W. Novotny, "Charge equalization for series connected battery strings," *IEEE Trans. Ind. Appl.*, vol. 31, no. 3, pp. 562–568, May/Jun. 1995.
- [22] A. Xu, S. Xie, and X. Liu, "Dynamic voltage equalization for series-connected ultracapacitors in EV/HEV applications," *IEEE Trans. Veh. Technol.*, vol. 58, no. 8, pp. 3981–3987, Oct. 2009.
- [23] L. Li, Z. Huang, H. Li, and H. Lu, "A high-efficiency voltage equalization scheme for supercapacitor energy storage system in renewable generation applications," *Sustainability*, vol. 8, no. 548, Jun. 2016.
- [24] J. Cao, N. Schofield, and A. Emadi, "Battery balancing methods: a comprehensive review," in Proc. *IEEE Veh. Power Propulsion Conf.*, pp. 1–6, Sep. 2008.
- [25] K. Z. Guo, Z. C. Bo, L. R. Gui, and C. S. Kang, "Comparison and evaluation of charge equalization technique for series connected batteries," in Proc. *IEEE Power Electron. Spec. Conf.*, pp. 1–6, Jun. 2006.
- [26] M. Uno and K. Tanaka, "Double-switch single-transformer cell voltage equalizer using a half-bridge inverter and voltage multiplier for series-connected supercapacitors," *IEEE Trans. Veh. Technol.*, vol. 61, no. 9, pp. 3920–3930, Nov. 2012.
- [27] M. Uno and A. Kukita, "Double-switch equalizer using parallel- or series-parallel-resonant inverter and voltage multiplier for series-connected supercapacitors," *IEEE Trans. Power Electron.*, vol. 29, no. 2, Feb. 2014, pp. 812–828.
- [28] M. Uno and A. Kukita, "Single-switch single-transformer cell voltage equalizer based on forward-flyback resonant inverter and voltage multiplier for series-connected energy storage cells," *IEEE Trans. Veh. Technol.*, vol. 63, no. 9, Nov. 2014, pp. 4232–4247.
- [29] M. Uno and K. Tanaka, "Single-switch cell voltage equalizer using multistacked buck-boost converters operating in discontinuous conduction mode for series-connected energy storage cells," *IEEE Trans. Veh. Technol.*, vol. 60, no. 8, pp. 3635–3645, Oct. 2011.
- [30] M. Uno and A. Kukita, "Two-switch voltage equalizer based on half-bridge converter with multi-stacked current doublers for series-connected batteries," in Proc. *IEEE ECCE-Asia, IPEC Hiroshima*, pp. 1444–1451, May 2014.
- [31] D. Andrea, Battery Management Systems for Large Lithium-Ion Battery Packs, London, United Kingdom: Artech House on Demand, 2010.
- [32] J. W. Kimball, B. T. Kuhn, and P. T. Krein, "Increased performance of battery packs by active equalization," in Proc. *IEEE Veh. Power Propulsion Conf.*, pp. 323–327, Sep. 2007.
- [33] S. West and P. T. Krein, "Equalization of valve-regulated lead-acid batteries: Issues and life test results," in Proc. *Int. Telecommun. Energy Conf.*, pp. 439–446, Sep. 2000.
- [34] M. Arias, J. Sebastian, M.M. Hernando, U. Viscarret, and I. Gil, "Practical application of the wave-trap concept in battery-cell equalizers," *IEEE Trans. Power Electron.*, vol. 30, no. 10, pp. 5616–5631, Oct. 2015.



**Masatoshi Uno** (M'06) was born in Japan in 1979. He received the B.E. degree in electronics engineering and the M.E. degree in electrical engineering from Doshisha University, Kyoto, Japan, and the Ph.D. degree in space and astronomical science from the Graduate University for Advanced Studies, Hayama, Japan, in 2002, 2004, and 2012, respectively.

In 2004, he joined the Japan Aerospace Exploration Agency, Sagami-hara, Japan, where he developed spacecraft power systems including battery, photovoltaic, and fuel cell systems. In 2014, he joined the Department of Electrical and Electronics Engineering, Ibaraki University, Ibaraki, Japan, where he is currently an Associate Professor of Electrical Engineering.

His research interests include switching power converters for renewable energy systems, life evaluation for supercapacitors and lithium-ion batteries, and development of spacecraft power systems. Dr. Uno is a member of the Institute of Electrical Engineers of Japan (IEEJ) and the Institute of Electronics, Information, and Communication Engineers (IEICE).



**Akio Kukita** was born in Japan in 1967. He received the B.E. degree in physics from Chuo University, Japan, in 1993.

From 1993 to 1996 and 1996 to 2008, he was with SEIKO Holdings Corporation and Ebara Corporation, respectively. Since 2008, he has been with Japan Aerospace Exploration Agency as a senior engineer. His recent work has focused on the development of spacecraft power systems.